https://doi.org/10.5194/egusphere-2022-1038
Preprint. Discussion started: 6 October 2022

Preconditioning of block onset in the Southern Hemisphere: a perspective from static stability

Li Dong[1], Hairu Ding[1,*], Guochun Shi[1,†], and Stephen J. Colucci[2]

[1]Department of Earth and Space Sciences, Academy for Advanced Interdisciplinary Studies, Southern University of Science and Technology, Shenzhen, Guangdong, China
[2]Department of Earth and Atmospheric Sciences, Cornell University, Ithaca, New York, USA
[*]Current affiliation: Max Planck Institute for Meteorology, Hamburg, Germany
[†]Current affiliation: University of Bern, Oescher Center for Climate Change Research, Bern, Switzerland

Correspondence: Li Dong (dongl@sustech.edu.cn)

Abstract. The horizontal and temporal variations of static stability prior to blocking onset are characterized through composite analysis of twenty blocking events in the Southern Hemisphere. It is found that, along with a low potential vorticity (PV) anomaly formation, a local minimum of static stability in the upper troposphere and on the tropopause is achieved over the block-onset region when blocking onset takes place. By partitioning the isentropic PV into the absolute vorticity and static stability contributions, it is found that they account for roughly 70 % and 30 % of low-PV anomaly formation over the block-onset region, respectively. A static stability budget analysis revealed that the decrease of static stability in the upper troposphere and on the tropopuase prior to blocking onset is attributable to horizontal advection of low static stability from subtropics to midlatitude as well as the stretching effect associated with upper-level convergence over the block-onset region, with the horizontal advection forcing being the primary contributor. On the other hand, the vertical advection of static stability tends to oppose the decreasing static stability through advecting more stable air downward such that it stabilizes the local air over the block-onset region. Furthermore, the direct effect of diabatic heating is negligible as its magnitude is generally an order of magnitude smaller than other effects in the static stability budget. Nevertheless, the indirect effect of diabatic heating, manifested as the advection of low static stability by diabatically forced upper-tropospheric outflow, greatly favors blocking onsets by destabilizing the air upstream block-onset region.

1 Introduction

Atmospheric blocking is commonly characterized as a stagnant large anticyclone or, sometimes, a cyclone-anticyclone dipole pattern that interrupts the eastward moving synoptic systems and thus leads to extreme weather conditions such as cold air outbreak, heat waves and drought. There have been many studies of mechanisms for atmospheric blocking onset and maintenance including instability theory (Frederiksen, 1982; Swanson, 2001), eddy-mean flow interactions (Green, 1977; Austin, 1980; Shutts, 1983; Illari, 1984; Mullen, 1987), the role of upstream explosive cyclogenesis (Tsou and Smith, 1990; Colucci and Alberta, 1996; Nakamura et al., 1997; Lupo and Smith, 1998) and Rossby wave breaking (Pelly and Hoskins, 2003; Masato et al., 2012).

https://doi.org/10.5194/egusphere-2022-1038
Preprint. Discussion started: 6 October 2022

Among many factors that collectively determine the onset of blocking, static stability, the vertical temperature stratification of the atmosphere, plays an important role in governing the stability of atmosphere within which baroclinic disturbances grow. In the framework of quasigeostrophic theory, static stability is assumed to be a function of height only, i.e. it is uniform on the horizontal surfaces. Nevertheless, the nature of the horizontal and temporal variability of the static stability could be important for understanding the onset of blocking. Based on the Eady linear growth rate (Eady, 1949), the baroclinic disturbances tend to grow rapidly in an atmosphere with low stability and vice versa. In the framework of baroclinic instability, Frederiksen (1982) employed a two-layer spherical quasi-geostrophic model to examine how cyclogenesis and blocking onset would occur given different static stability. It is found that the fastest growing perturbations with monopole structure, which resemble cyclogenesis, take place in a relatively unstable mean flow, whereas perturbations with high-low dipole structure, which resemble blocking, occur in a less unstable flow. Smith and Tsou (1988) characterized the static stability variations during the development of an intense extratropical cyclone through a generalized height tendency equation and found that static stability plays a dual role in a synoptic-scale wave development, namely, it not only determines the stability condition of the mean flow, but also acts as a forcing term on the height tendency field through the vertical advection of static stability. Moreover, Smith and Tsou (1988) showed that the static stability in the lower troposphere reached its minimum at the initial stage of cyclone development and then increased during the rapid cyclone intensification process. This finding is consistent with Frederiksen (1982) in that the baroclinic disturbances are favored to grow in a background flow with relatively low static stability.

So far there have been numerous studies on characterizing static stability (Frierson, 2006; Frierson and Davis, 2011; Grise et al., 2010; O'Gorman, 2011; Erler and Wirth, 2011), but most of these studies are focused on the global structure of static stability. Duran and Molinari (2019) used a static stability budget equation to extensively examine the upper-level static stability variations during the rapid intensification of a simulated tropical cyclone. Nevertheless, to the best of the authors' knowledge, no studies have been carried out yet to systematically quantify static stability variations associated with blocking onset. In addition, based on the definition of isentropic potential vorticity (PV) proposed by Hoskins et al. (1985), the change of PV on isentropic surfaces is due to the changes of absolute vorticity and static stability, respectively. When blocking takes place, the formation of low-PV anomaly over the block-onset region can be attributed to either the low absolute vorticity anomaly or low static stability anomaly. However, how much the low static stability anomaly contributes to the low-PV formation over the block-onset region has not been exclusively quantified so far. Hence, in this study, we intend to address three questions: (1) What are the key characteristics of static stability evolutions during blocking onset? (2) How much does static stability contribute to initiate blocking onset? and (3) What causes the static stability variations during blocking onset? We will attempt to answer these questions through both single and composite case studies of blocking onsets. Given that the influence of continent distribution is relatively small in the Southern Hemisphere (SH), compared to the Northern Hemisphere (NH), we intend to focus on the SH in this study for the purpose of simplicity.

Regarding the above question (3), we are particularly interested in addressing the influence of latent heating on static stability variations during blocking onset. Recent studies have shown that moist dynamics is equally important to blocking onset, relative to the dry dynamics, in that the ascending motion due to the lower-level cloud-associated latent heating release results

https://doi.org/10.5194/egusphere-2022-1038
Preprint. Discussion started: 6 October 2022

in a cross-isentropic ascent and strong divergent outflow at upper troposphere and tropopause (Pfahl et al., 2015; Steinfeld and Pfahl, 2019). These cross-isentropic ascending air parcels experience substantial PV modifications by latent heating and generate a net vertical transport of anticyclonic PV anomalies in the upper troposphere (Hoskins et al., 1985; Wernli and Davies, 1997; Methven, 2015). These injected anticyclonic PV anomalies are usually associated with tropopause folds, downstream ridge amplification, and Rossby wave modulation which are closely linked to blocking onset (Grams et al., 2011; Teubler and Riemer, 2016; Madonna et al., 2014). The injection of diabatically processed anticyclonic PV is usually interpreted as the direct effect of latent heat release upon the upper-level flow whereas the poleward advection of anticyclonic PV by the diabatically driven outflow is interpreted as the indirect effect of latent heating (Croci-Maspoli and Davies, 2009; Quinting and Reeder, 2017; Parker et al., 2013; Grams et al., 2011; Grams and Archambault, 2016; Teubler and Riemer, 2016). The warm conveyor belt (WCB) of extratropical cyclones, namely the intense ascending moist airflows rising from lower troposphere into upper troposphere while moving polewards, is the most typical weather system that is associated with predominant latent heat release over the midlatitudes (Madonna et al., 2014; Wernli, 1997). In addition, other weather systems such as predecessor rain events (PREs) studied by Grams and Archambault (2016) and the extratropical transition (ET) of tropical cyclones (Grams and Archambault, 2016; Grams et al., 2013, 2011; Riemer et al., 2008; Archambault et al., 2013; Bosart and Lackmann, 1997) are also particularly associated with strong latent heat release. Hence, it is worthwhile to investigate the role of latent heating in blocking onset from the perspective of static stability in the present study.

The remainder of this study is organized as follows. A detailed explanation of a static stability tendency equation is presented in section 2. The blocking detection criteria and data sets used for this study are described in section 3. In section 4, the synoptic evolutions of a selected 1999 July blocking event and composite blocking events prior to block onset are depicted through the isentropic PV (IPV) perspective. In section 5, characteristics of static stability evolution associated with blocking onset are presented. Section 6 is focused on static stability budget analysis using the static stability tendency equation. Finally, overall discussion and conclusions are given in section 7.

2 Diagnostic model

Following Bluestein (1992), an adiabatic and frictionless quasigeostrophic diagnostic equation for the geopotential height (z) tendency field can be written as below

$$\left[\nabla_p^2 + f_0^2 \frac{\partial}{\partial p}\left(\frac{1}{\sigma}\frac{\partial}{\partial p}\right)\right]\left(\frac{\partial z}{\partial t}\right) = -\left(\frac{f_0}{g}\right)\mathbf{V_g}\cdot\nabla_p(\zeta_g + f) - f_0^2\frac{\partial}{\partial p}\left[\left(\frac{1}{\sigma}\right)\mathbf{V_g}\cdot\nabla_p\left(\frac{\partial z}{\partial p}\right)\right]. \quad (1)$$

https://doi.org/10.5194/egusphere-2022-1038
Preprint. Discussion started: 6 October 2022

Here $\mathbf{V_g}$ is the geostrophic wind, ∇_p is the gradient operator in spherical coordinates on a constant pressure (p) surface, f_0 is the Coriolis parameter, g is gravity, and σ is the static stability parameter written as

$$\sigma = -\left(\frac{\alpha}{\theta}\right)\frac{\partial\theta}{\partial p}, \tag{2}$$

or

$$\sigma = -\frac{RT}{p\theta}\frac{\partial\theta}{\partial p} = -\frac{R}{p}\left[\left(\frac{p}{1000}\right)^{\frac{R}{c_p}}\right]\frac{\partial\theta}{\partial p} \tag{3}$$

which is assumed to vary with pressure only. Here α is specific volume and R is ideal gas constant. It is readily clear that the static stability parameter influences the rate of development of synoptic-scale systems through its appearance in both a forcing term as well as the operator in front of height tendency.

Starting from the thermodynamic equation, Bluestein (1992) derived the static stability tendency equation as follows

$$\frac{\partial}{\partial t}\left(-\frac{\partial\theta}{\partial p}\right) = \underbrace{-\frac{\partial}{\partial p}\left(-\mathbf{V}\cdot\nabla_p\theta\right)}_{(1)}\underbrace{-\omega\frac{\partial}{\partial p}\left(-\frac{\partial\theta}{\partial p}\right)}_{(2)}\underbrace{-\delta\frac{\partial\theta}{\partial p}}_{(3)}\underbrace{-\frac{\partial}{\partial p}\left(\frac{\theta}{C_pT}\frac{dQ}{dt}\right)}_{(4)}, \tag{4}$$

where $\delta = \frac{\partial u}{\partial x} + \frac{\partial v}{\partial y}$. In Eq. (4), the left hand side is the static stability tendency term which represents the local change of static stability. Since the static stability parameter σ is $\frac{\partial\theta}{\partial p}$ multiplied by a factor $-\frac{R}{p}\left[\left(\frac{p}{1000}\right)^{\frac{R}{c_p}}\right]$, Eq. (4) can be interpreted as the isobaric tendency equation of static stability. On the right hand side, term 1 is the differential temperature advection, term 2 is the vertical advection of static stability, term 3 is the local change of static stability induced by vertical stretching or shrinking of an air column, and term 4 is the differential diabatic heating.

Based on the previous discussion regarding the direct and indirect effects of the latent heat release to blocking onset, we decompose the wind vector $\mathbf{V}$ into rotational wind $\mathbf{V_r}$ and divergent wind $\mathbf{V_d}$. Thus the the differential temperature advection (term 1) can be rewritten as

$$-\frac{\partial}{\partial p}\left(-\mathbf{V}\cdot\nabla_p\theta\right) = -\frac{\partial}{\partial p}\left(-\mathbf{V_r}\cdot\nabla_p\theta\right) - \frac{\partial}{\partial p}\left(-\mathbf{V_d}\cdot\nabla_p\theta\right) \tag{5}$$

where the first term on the right hand side represents the differential temperature advection by the rotational wind and the second term by the divergent wind.

Hence, Eq. (4) can be further expanded as follows

$$\frac{\partial}{\partial t}\left(-\frac{\partial\theta}{\partial p}\right) = \underbrace{-\frac{\partial}{\partial p}\left(-\mathbf{V_r}\cdot\nabla_p\theta\right)}_{(1)} \underbrace{-\frac{\partial}{\partial p}\left(-\mathbf{V_d}\cdot\nabla_p\theta\right)}_{(2)}\underbrace{-\omega\frac{\partial}{\partial p}\left(-\frac{\partial\theta}{\partial p}\right)}_{(3)}\underbrace{-\delta\frac{\partial\theta}{\partial p}}_{(4)}\underbrace{-\frac{\partial}{\partial p}\left(\frac{\theta}{C_pT}\frac{dQ}{dt}\right)}_{(5)} \tag{6}$$

Equation (6) shows that a local change of static stability may be caused by horizontal and vertical advection of static stability through terms 1, 2 and 3 respectively. Note that these terms can only move static stability from one place to another, but they can neither create or destroy stability (Bluestein, 1992). However, static stability may be locally generated or destroyed through vertical shrinking or stretching effect of an air column, as represented in term 4. It can also be generated or destroyed locally through the diabatic heating effect as shown in term 5. Hence terms from 1 through 5 in Eq. (6) work collectively to alter the local change of static stability. The results of detailed static stability budget analysis will be presented in Section 6.

https://doi.org/10.5194/egusphere-2022-1038
Preprint. Discussion started: 6 October 2022

3 Data

The Modern-Era Retrospective analysis for Research and Applications, Version 2 (MERRA-2) from NASA Global Modeling and Assimilation Office (GMAO) is used in this study. The data is on a $0.5^o \times 0.625^o$ regular grid with 42 vertical levels for the period 1980-2016. Specifically, the 3-hourly instantaneous pressure-level meteorological fields are utilized in the following computation, except for the diabatic heating, which is based on the 3-hourly time-averaged pressure-level temperature tendencies.

A variety of blocking detection approaches have been utilized by previous studies of blocking onsets, with each approach having pros and cons as detailed in Barnes et al. (2012). Following Steinfeld and Pfahl (2019), we detected blocking based on an absolute geopotential height reversal-based (AGP) blocking index (Tibaldi and Molteni, 1990) and PV-anomaly-based (APV) blocking index (Pelly and Hoskins, 2003; Schwierz et al., 2004), respectively. The AGP blocking index primarily detects the flank of the anticyclonic circulation anomalies where westerly winds are reversed, while the APV blocking index focuses on the center of the anomalous anticyclonic circulation. Specifically, we used a modified version of the AGP blocking index from Tibaldi and Molteni (1990), with details of the detection algorithm described in Watson and Colucci (2002) where blocking is defined as a negative zonal index persistent for at least five days and spanning at least 20 degrees of longitude. Here the negative zonal index is defined as 500 hPa geopotential heights being higher at 60^oS than at 40^oS. The first day on which this blocking index criterion is met is defined as block onset for a specific blocking event. Furthermore, in order to ensure that these detected blocking cases also meet the APV blocking index, we screened these blocking cases against PV-anomaly based blocking criteria. Finally, 20 typical blocking cases are selected among all blocking cases detected based on the combination of the AGP and APV blocking indices during 1980-2010. Table 1 lists the selected blocking cases with the corresponding block-onset date and western boundary of the block-onset region. Detailed description of the synoptic evolutions of a selected blocking case and composite blocking cases will be presented in the following section. Note that in this study PV values are multiplied by -1 in the SH such that the low-PV anomaly concept associated with blocking onset in the NH is equally applied to the SH.

https://doi.org/10.5194/egusphere-2022-1038
Preprint. Discussion started: 6 October 2022

Table 1. Selected 20 blocking events in the SH during 1980-2010.

Case ID	block-onset day	west boundary of block-onset region
1	06/09/1986	160^o W
2	06/24/1986	167.5^o W
3	07/27/1986	137.5^o W
4	06/20/1987	135^o W
5	07/05/1987	127.5^o W
6	08/15/1988	112.5^o W
7	05/20/1991	127.5^o W
8	06/15/1992	155^o W
9	05/29/1994	172.5^o W
10	09/17/1994	165^o W
11	07/25/1999	167.5^o W
12	07/11/2000	68^o W
13	08/23/2000	135^o E
14	06/09/2002	122^o W
15	08/11/2002	138^o W
16	03/17/2003	134^o W
17	08/27/2003	177^o W
18	06/01/2005	152^o W
19	06/19/2006	142 ^{o} W
20	07/23/2008	166^o E

4 Synoptic evolution of blocking events

In order to better understand variations in static stability associated with block onset, we follow Hoskins et al. (1985) to examine the blocking evolution from the perspective of IPV which contains both dynamic and thermodynamic processes as shown below.

$$IPV = -g(\zeta_\theta + f)\frac{\partial \theta}{\partial p}, \tag{7}$$

where ζ_θ is the relative vorticity on the isentropic surfaces. Since IPV is conserved on isentropic surfaces for adiabatic and frictionless processes, it can be used as a tracer to keep track of the air parcel. From Eq. (7), it is readily clear that IPV can be altered through changes in absolute vorticity or static stability.

Generally, the stratosphere is characterized by large IPV values because of high static stability in the stratosphere whereas the troposphere is distinguished by low IPV values due to relatively low static stability in the troposphere. For a typical isentropic

https://doi.org/10.5194/egusphere-2022-1038
Preprint. Discussion started: 6 October 2022

surface on which the troposphere and stratosphere are intersected, such as 320 K surface, generally, the high latitudes are featured with stratospheric high IPV but the subtropics featured with tropospheric low IPV. Commonly, relative minima of IPV that originated from the subtropics can extrude poleward and may become a cut-off ridge that is closely associated with a blocking anticyclone (Hoskins et al., 1985). This is also known as a PV streamer according to the previous studies (Appenzeller and Davies, 1992; Nielsen-Gammon, 2001; Wernli and Sprenger, 2007). Next, we will present the synoptic evolutions of a selected blocking event as well as 20 blocking events composite from the perspective of IPV.

4.1 July 1999 blocking case

Figure 1 depicts the evolution of the July 1999 blocking case for the five days prior to block onset through the block-onset day. A classic dipole blocking structure that resembles the one described by Rex (1950) is readily observed on 25 July, which is the objectively defined block-onset day. This blocking case lasted for six days through 30 July (not shown), when the anticyclone of the dipole started to retrogress and, in a consequence, the blocking structure dissolved. As this case was also extensively studied by Dong and Colucci (2005), to which the reader is referred for a detailed synoptic description.

https://doi.org/10.5194/egusphere-2022-1038
Preprint. Discussion started: 6 October 2022

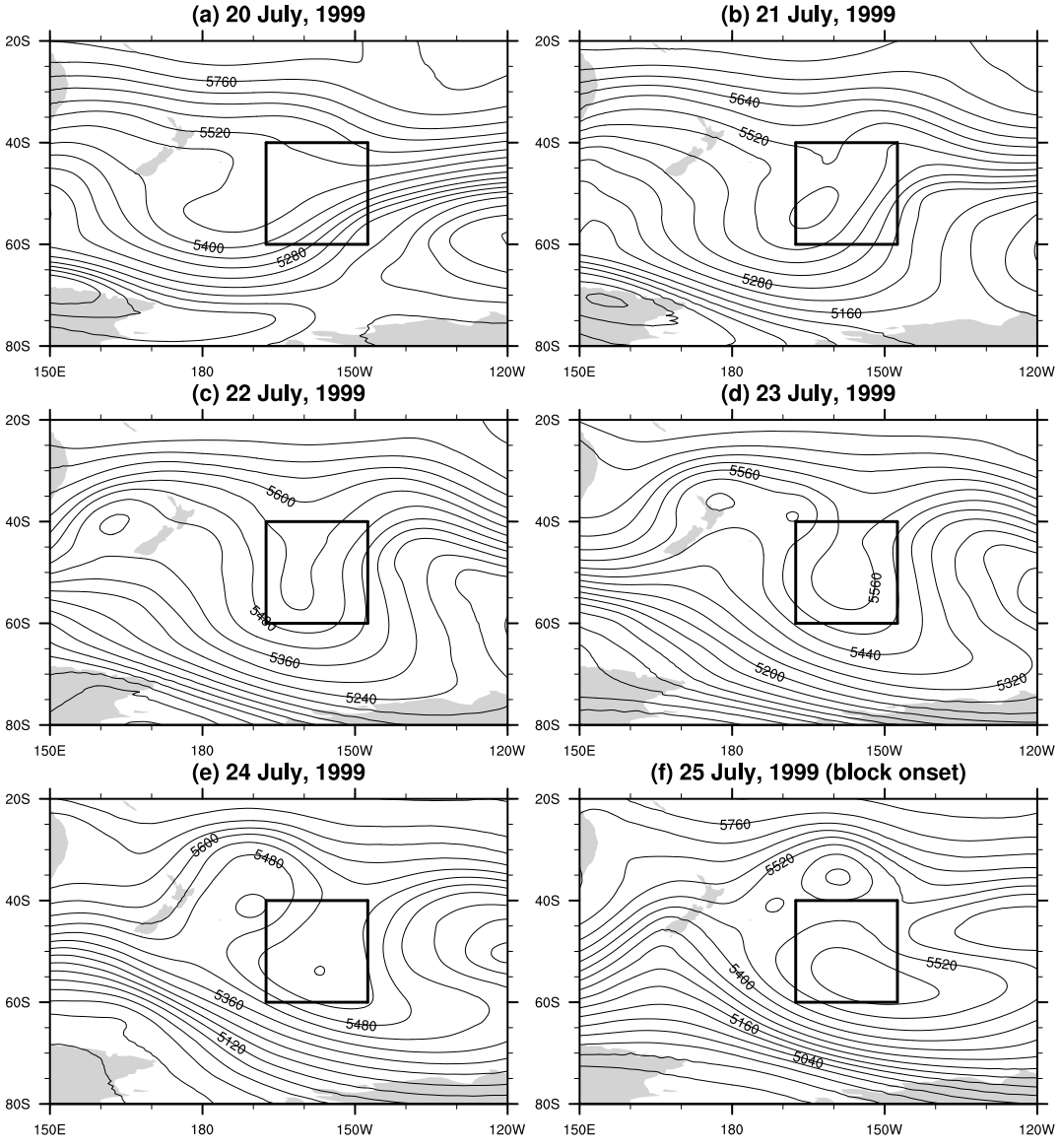

Figure 1. 500 hPa height analyses of July 20-25, 1999. The block-onset day is July 25, 1999. The block-onset region is outlined by a rectangle. The contour interval is 60 m.

Figure 2 depicts the IPV anomaly evolution on 320 K isentropic surface of the July 1999 blocking event for the 5-day pre-blocking period through the block-onset day. Here the IPV anomaly is computed as the difference between the analyzed IPV and the long-term mean IPV. On 22 July, a low IPV anomaly started to extrude poleward and became a cut-off low IPV anomaly on the following day. On 24 July, one day prior to block onset, an upstream new low IPV tongue started to extend poleward and then merged with the stranded cut-off low IPV anomaly on the block-onset day. The markedly low IPV anomaly

https://doi.org/10.5194/egusphere-2022-1038
Preprint. Discussion started: 6 October 2022

dominant over the block-onset region manifests as block onset as shown in Fig. 1f, with the center of the low IPV anomaly located around (160^o W, 65^o S). It is readily evident that strong northwesterly winds upstream the low IPV anomaly center are largely effective in advecting low IPV air poleward. Note that the block-onset region outlined in Fig. 1 is based on the AGP blocking index, which is slightly equatoward of the low IPV anomaly center.

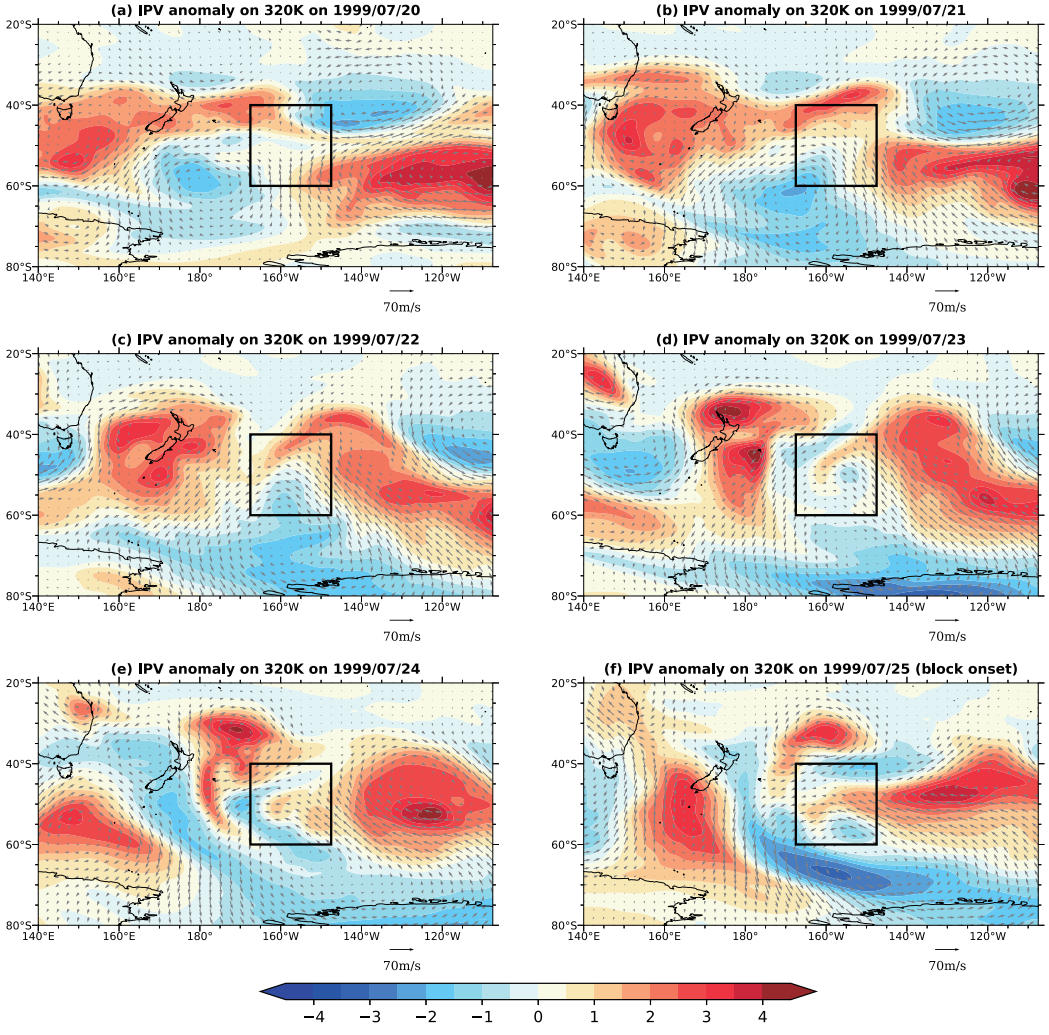

Figure 2. IPV anomaly on 320 K isentropic surface for July 20-25, 1999. The contour interval is 1.0 PVU, where 1 PVU=10^{-6} K m^2 kg^{-1} s^{-1}. The horizontal velocity vectors are shown in arrows with the magnitude scale located on the lower right corner in unit of m s^{-1}. The block-onset region is outlined with a rectangle.

https://doi.org/10.5194/egusphere-2022-1038
Preprint. Discussion started: 6 October 2022

Figure 3 shows a vertical cross section of PV anomaly and isentropes, taken over the blocking center, on pressure surfaces for the block-onset day of the July 1999 blocking event. The black dark dashed contour is the 2 PVU surface that is commonly used to represent the location of the dynamical tropopause (Hoskins, 1997). It is evident that the dynamical tropopause experiences undulations near the positive and negative PV anomaly centers. Over the block-onset region, the dynamical tropopause is elevated due to a striking low-PV anomaly structure whereas the dynamical tropopause sinks over upstream of the block-onset region due to a strong high-PV anomaly associated with the upstream cyclone.

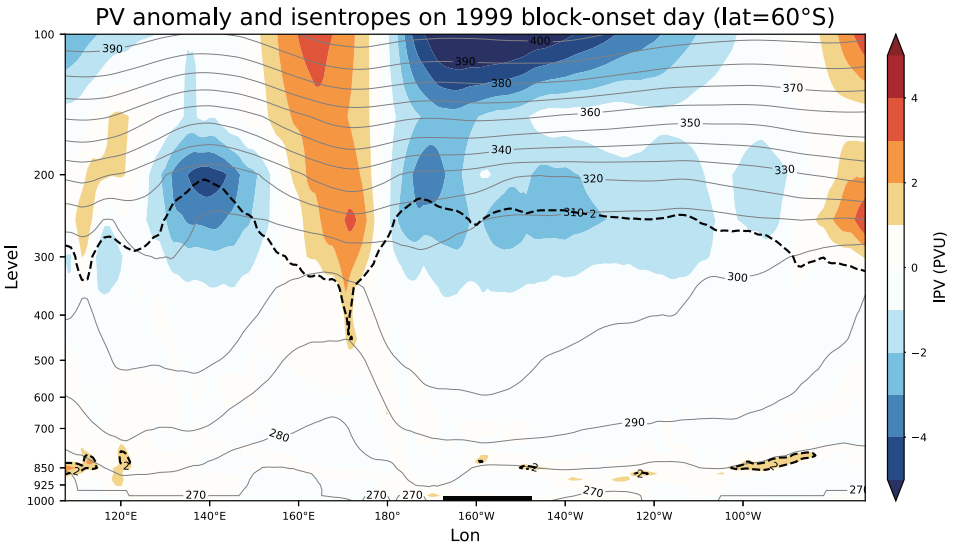

Figure 3. Vertical cross section of PV anomaly (shade), isentropes (K) (thin grey line) and PV=2 PVU contour (thick black dash line) for July 25, 1999 (block onset day). The cross section is taken at 60 ^{o} S. The block-onset region is highlighted with a narrow black rectangle along the longitude axis.

4.2 Composite blocking

The selected 20 SH blocking events during 1980-2010 are analyzed in a composite way such that the composite results are presented in a block onset relative coordinate where the longitude is pseudo longitude and the block-onset region is centered at 180^o W.

In a similar fashion to the July 1999 blocking case, the 500 hPa composite height field started to split into poleward and equatorward branches near block-onset region on day-5 as shown in Fig. 4a. The poleward branch continued to amplify on the following days and a dominant anticyclonic ridge was resulted on one day prior to block onset, as shown in Fig. 4e. On the block-onset day, the anticyclonic structure continued to grow poleward while a cyclonic structure formed equatorward. This quasi-dipole pattern in the blocking composite considerably resembles that of the July 1999 blocking event on the block-onset day as shown in Fig. 1f, with the latter featuring greater amplitudes.

https://doi.org/10.5194/egusphere-2022-1038
Preprint. Discussion started: 6 October 2022

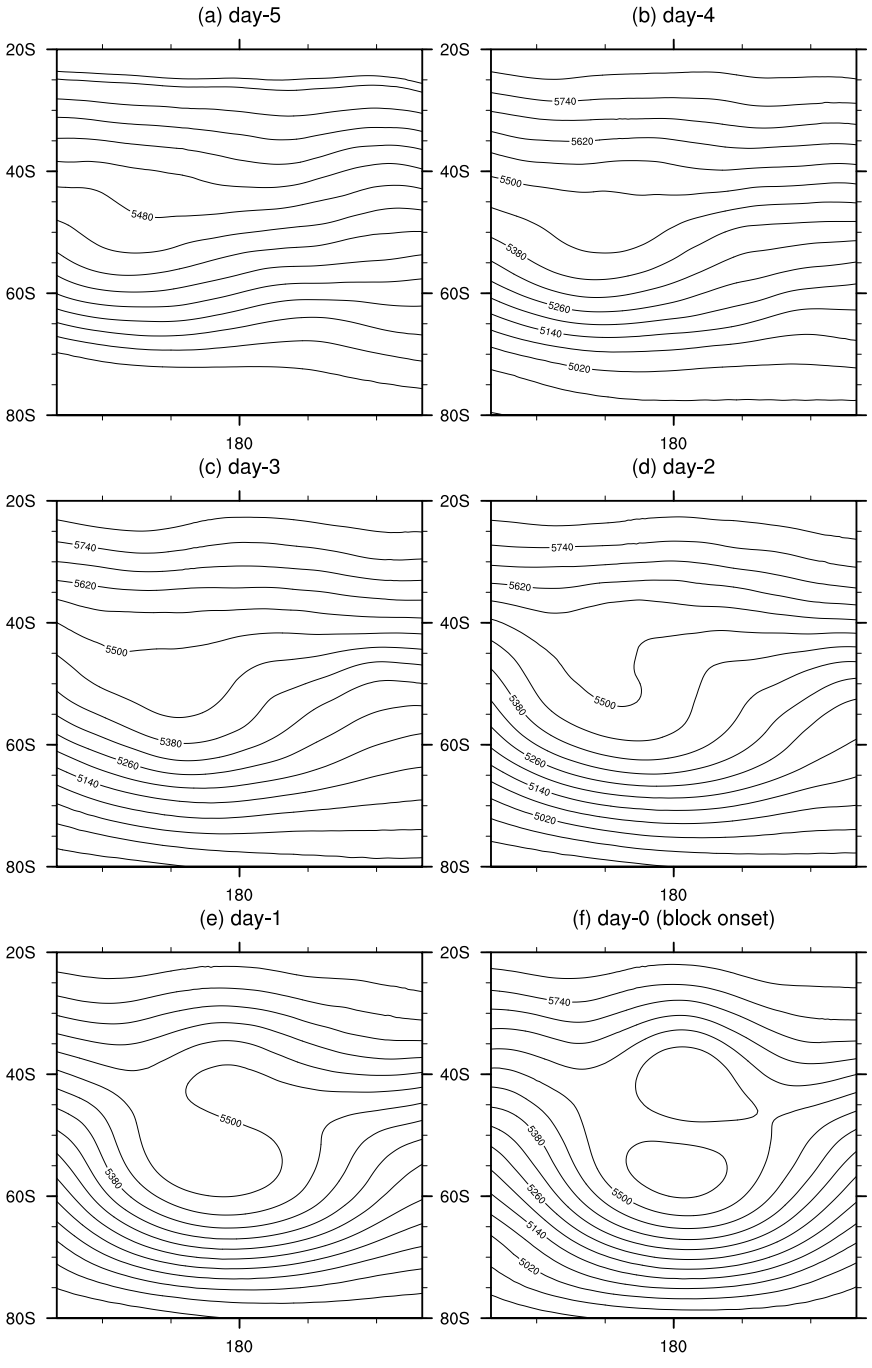

Figure 4. Same as in Fig 1 except for composite blocking events during 5-day pre-blocking period and block-onset day. The longitude is a pseudo longitude along which the block-onset region is centered at 180 ^{o} W.

https://doi.org/10.5194/egusphere-2022-1038
Preprint. Discussion started: 6 October 2022

In terms of PV anomaly evolution on the 320 K surface as shown in Fig. 5, the composite results show a very similar sequence as seen in the July 1999 blocking case, featuring a low IPV anomaly, originated from subtropics, gradually penetrating poleward prior to block onset. When the low PV anomaly further extrudes poleward while maintaining its strong anticyclonic circulation, it usually becomes a cut-off low PV anomaly. To some extent, this process is similar to PV wave breaking during which the planetary waves are amplified such that they become too large to be maintained (Pelly and Hoskins, 2003).

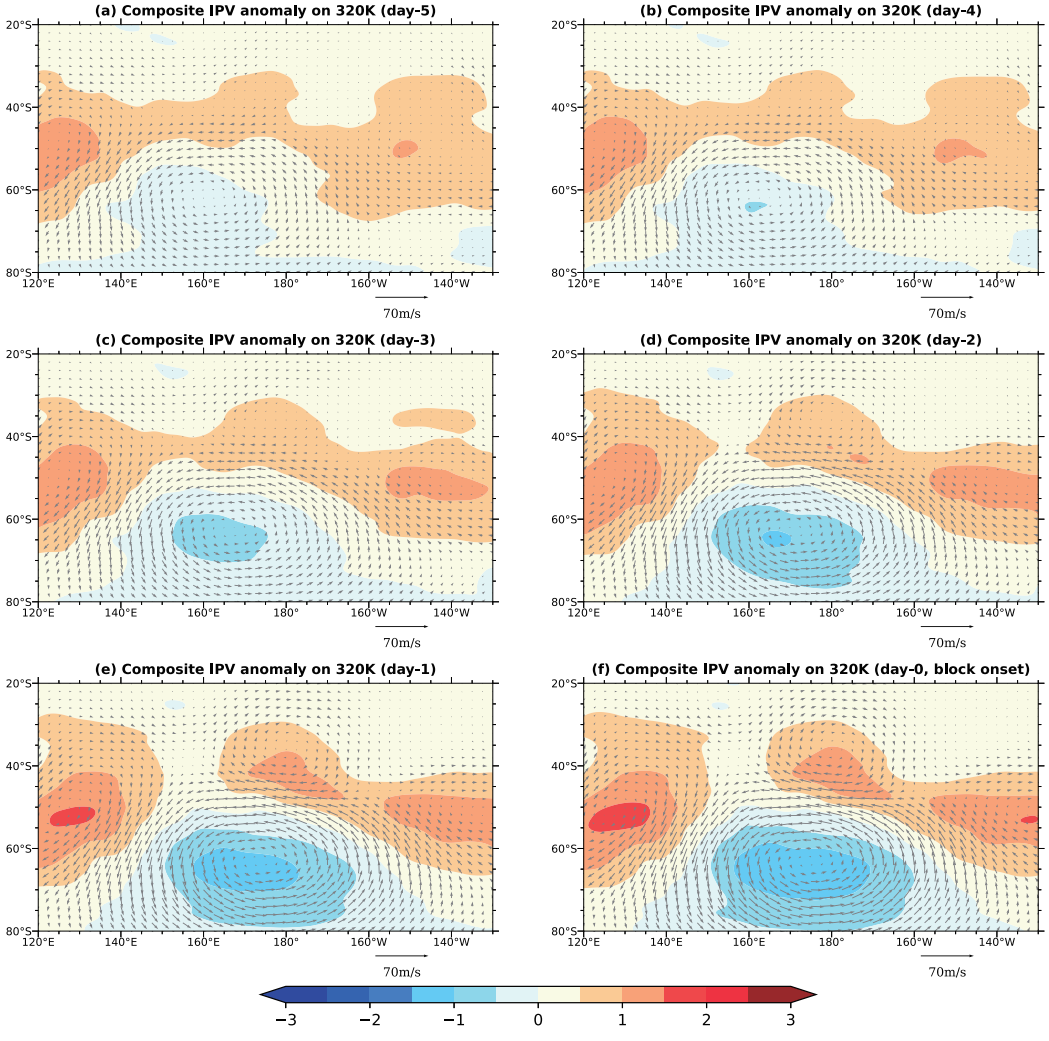

Figure 5. Same as in Fig. 2 except for composite blocking events during 5-day pre-blocking period and block-onset day.

https://doi.org/10.5194/egusphere-2022-1038
Preprint. Discussion started: 6 October 2022

Figure 6 shows the vertical cross section of PV anomaly and isentropes on pressure surfaces for the composite block-onset day. It is evident that over the composite block-onset region, which is centered at 180^o W, the upper-troposphere is characterized by a predominant low-PV anomaly, resulting in a well-elevated tropopause over the composite block-onset region. The cyclones upstream and downstream of the composite block-onset region are both associated with high-PV anomaly and sinking tropopause, with the former featuring a greater magnitude. Nevertheless, in terms of the PV anomaly intensity, the composite blocking structure features a stronger PV anomaly pattern, relative to the composite upstream cyclones.

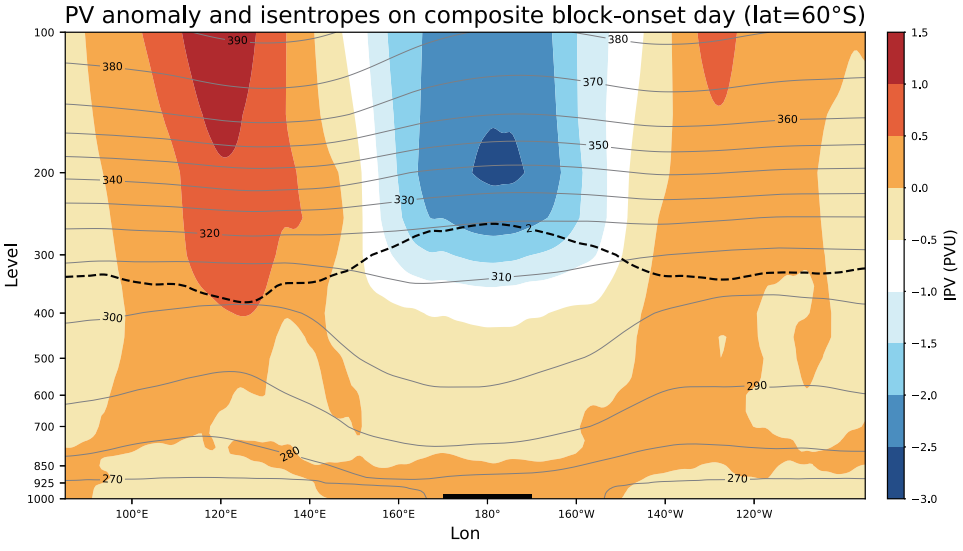

Figure 6. Same as in Fig. 3 except for the composite blocking events. The longitude axis is pseudo longitude. The composite block onset region is centered at 180^o W.

5 Static stability characterization

5.1 Climatology of static stability

Before we proceed to discuss the variations of static stability associated with blocking onsets, first, we will present the global climatology of static stability. Figure 7 displays the long-term mean static stability parameter σ, as shown in Eq. (3), at 300 hPa for SH winter (JJA) and summer (DJF) respectively. Given 300 hPa is near the tropopause, it is evident that the subtropics are dominated by tropospheric air associated with relatively low static stability while the high latitudes are dominated by stratospheric air characterized by large static stability, as depicted in Fig. 7. This is consistent with Grise et al. (2010) who identified a minimum in static stability in the tropical upper troposphere. In Fig. 7, the latitude zone where the troposphere intersects stratosphere is characterized with strong meridional gradient of static stability. As the season evolves from winter to

https://doi.org/10.5194/egusphere-2022-1038
Preprint. Discussion started: 6 October 2022

summer in the SH, this zone gradually migrates poleward since tropopause is higher over tropics in summer than winter and there is a wider tropical latitude band that is characterized by tropospheric air at 300 hPa.

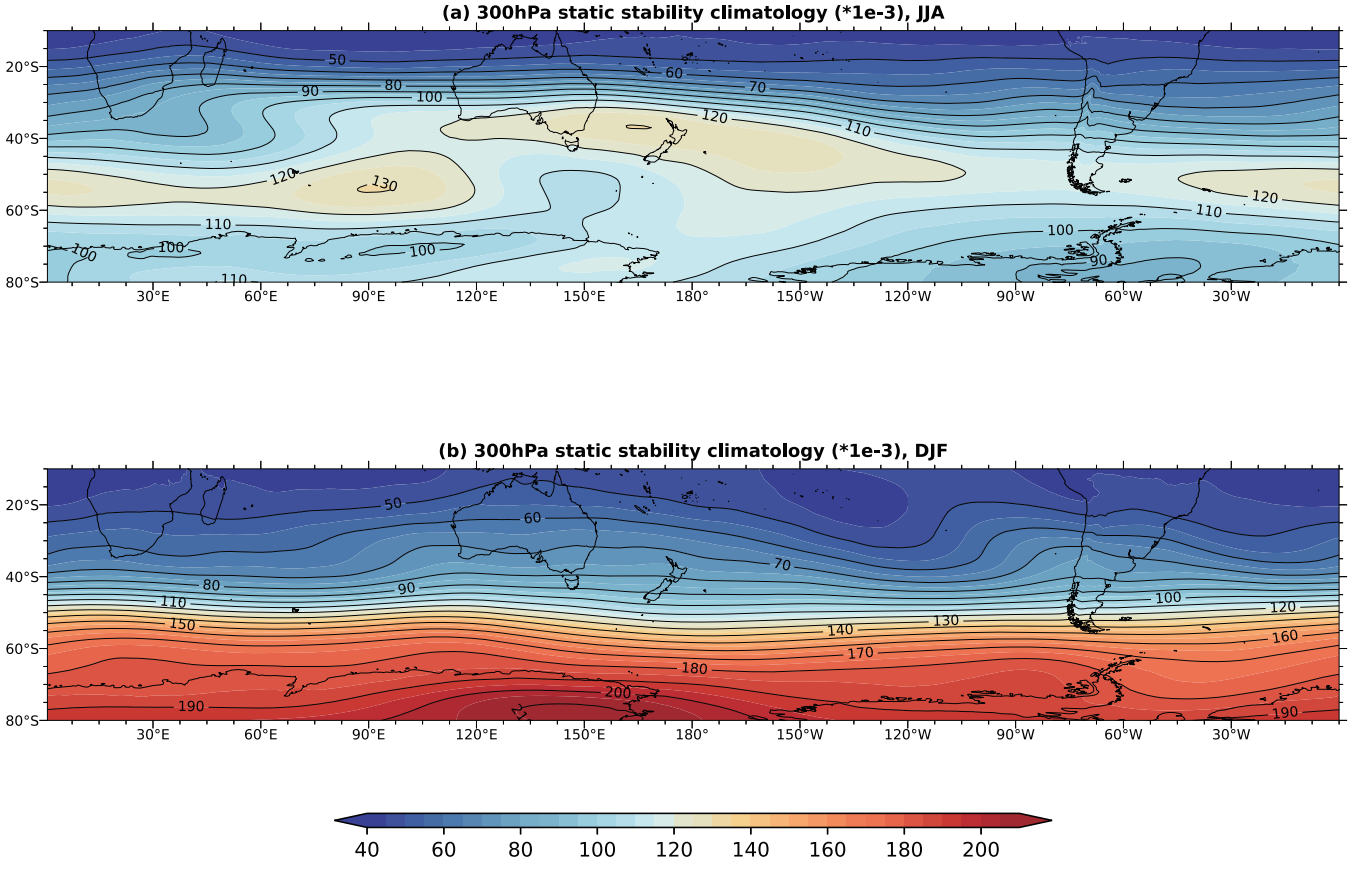

Figure 7. Climatology of 300 hPa static stability (1981-2010) in the Southern Hemisphere during JJA in (a) and DJF in (b). The contour interval is 10×10^{-3} m^2 s^{-2} hPa^{-2}.

5.2 Blocking-associated static stability

Figure 8 shows the sequence of 300 hPa static stability anomaly overlaid with 500 hPa geopotential heights during the 5-day pre-blocking period and block-onset day for the July 1999 blocking event. Here the static stability anomaly is computed as the difference between the analyzed static stability and the long-term mean static stability. The block-onset day is July 25, 1999. On July 20, a local minimum of static stability shows up on the lower left corner of the block-onset region, associated with the

https://doi.org/10.5194/egusphere-2022-1038
Preprint. Discussion started: 6 October 2022

anticyclonic ridge approaching to the block-onset region. As the ridge amplifies on the following day, the local minimum of static stability continues to intensify. On July 22, in addition to the existing local minimum of static stability on the poleward side of the block-onset region, another local stability minimum emerges, accompanying a ridge on the equatorward side of the block-onset region. On July 23, these two local stability minima start to merge and stay through the block-onset day. The evolution of the static stability minima is accompanied by the blocking anticyclone formation. Here the evolution of upper-troposphere static stability prior to block onset bears a close resemblance to the IPV evolution, as shown in Fig. 2, in that both quantities feature a local minimum over the block-onset region approaching the block-onset day.

The characteristic evolution of static stability is more evident from the sequence of composite static stability anomaly, shown in Fig. 9, as a relatively weak tongue of low static stability gradually dips poleward as a ridge starts to amplify upstream block-onset region five days before the block-onset day. Recall from the climatology of static stability discussed above, it is clear that the low static stability associated with tropospheric air in subtropics is advected poleward to the midlatitudes. For the following a few days, the low static stability tongue is further intensified and propagates into the block-onset region. On the block-onset day, the low static stability reaches its local minimum over the block-onset region. Once again, the evolution of composite upper-troposphere static stability closely resembles that of the composite IPV anomaly, as shown in Fig. 5, with both quantities reaching a local minimum over the block-onset region on the block-onset day.

5.3 Attributions of IPV changes to static stability

In order to explicitly quantify the relative contribution of static stability variations to IPV changes, we derive the local change of IPV attributable to the local changes of static stability and absolute vorticity, respectively, as follows.

Eq. (7) may be schematically written as

$$IPV = A \cdot B, \tag{8}$$

where $A = g(\zeta_\theta + f)$ and $B = -\frac{\partial \theta}{\partial p}$.

By taking the derivative over both sides of Eq. (8), it becomes

$$\begin{aligned} \delta(IPV) &= \delta(A \cdot B) \\ &= A\delta B + B\delta A \end{aligned} \tag{9}$$

After both sides of Eq. (9) are divided by IPV, it becomes

$$\begin{aligned} \frac{\delta(IPV)}{IPV} &= \frac{A\delta B}{AB} + \frac{B\delta A}{AB} \\ &= \frac{\delta B}{B} + \frac{\delta A}{A} \end{aligned} \tag{10}$$

Hence, Eq. (10) readily shows that the relative change of IPV is attributed to the relative changes of static stability and absolute vorticity, respectively. Here the local change of IPV, absolute vorticity and static stability, i.e. $\delta(IPV)$, δA and δB, can be approximately estimated as the anomalous departure from their corresponding long-term mean values. Therefore, the relative change is estimated as the anomaly values divided by the analyzed values.

https://doi.org/10.5194/egusphere-2022-1038
Preprint. Discussion started: 6 October 2022

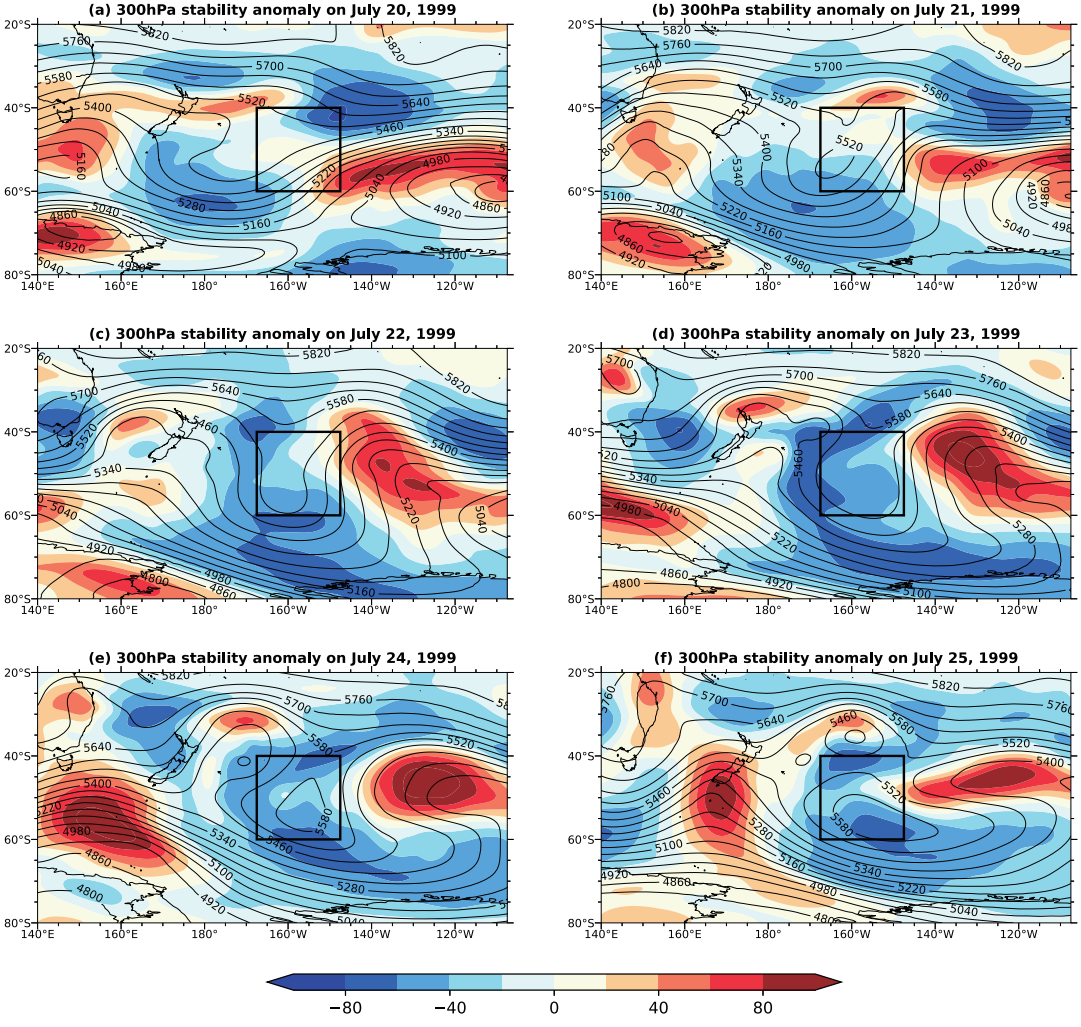

Figure 8. 300 hPa static stability anomaly (shade) for the blocking event during July 20-25, 1999, in unit of 10^{-3} $\mathrm{m^2\ s^{-2}\ hPa^{-2}}$, overlaid with 500 hPa geopotential height (contour) in interval of 60 m. The block-onset day is July 25, 1999. The block-onset region is outlined with the rectangle.

The Eq. (10) is applied to both the July 1999 blocking case and the composite blocking cases, as shown in Fig. 10 and Fig. 11, respectively. Both figures demonstrate that, in general, the local decrease of IPV is dominant over the block-onset region, with the local decrease of absolute vorticity accounting for 70 % of IPV change and the local decrease of static stability accounting for 30 % of IPV change. In other words, the formation of low-PV anomaly over block region is determined jointly by absolute vorticity and static stability. Hence, the investigation of the local change of static stability would shed light on understanding the dynamic evolution of blocking events.

https://doi.org/10.5194/egusphere-2022-1038
Preprint. Discussion started: 6 October 2022

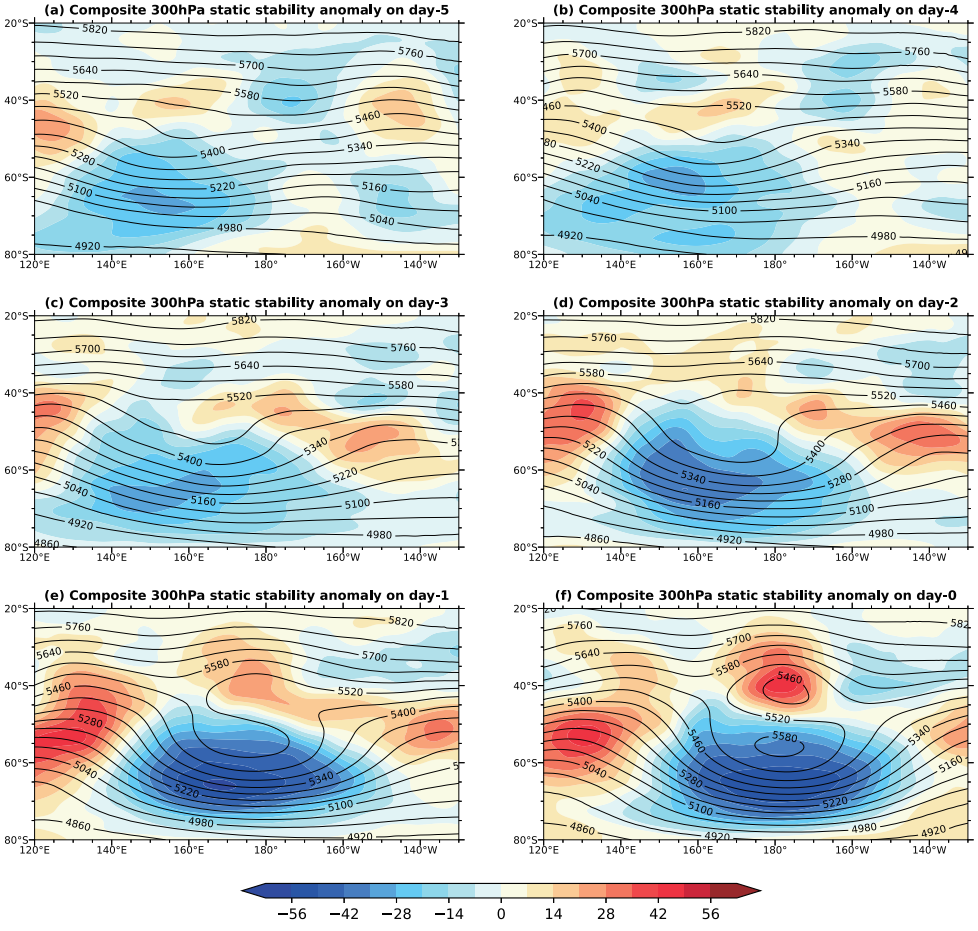

Figure 9. Same as in Fig. 8 except for the composite blocking events during 5-day pre-blocking period and block-onset day.

https://doi.org/10.5194/egusphere-2022-1038
Preprint. Discussion started: 6 October 2022

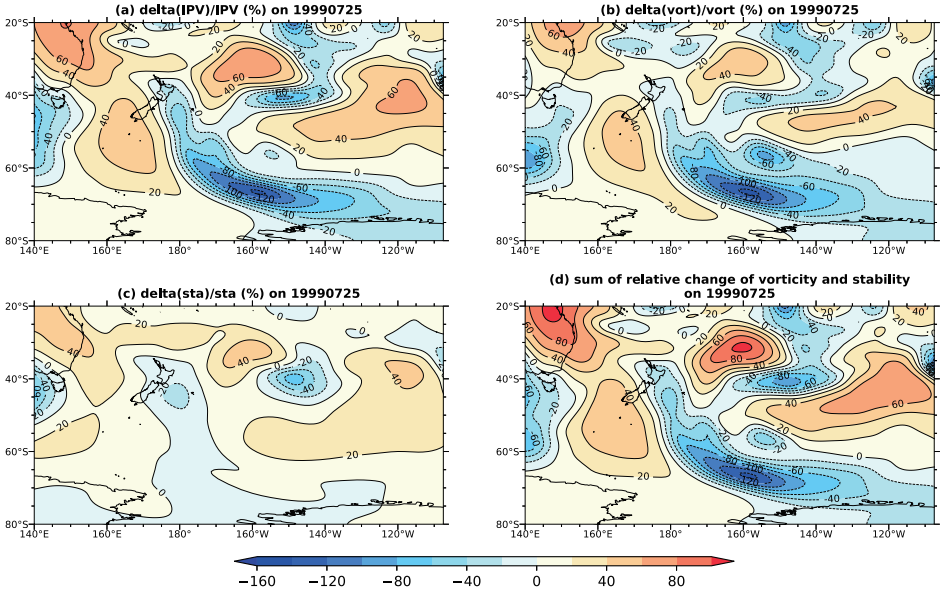

Figure 10. The relative change (in percentage) of IPV in (a), absolute vorticity in (b), static stability in (c) and the sum of (b) and (c) as shown in (d) on 320 K for the block-onset day, July 25, 1999.

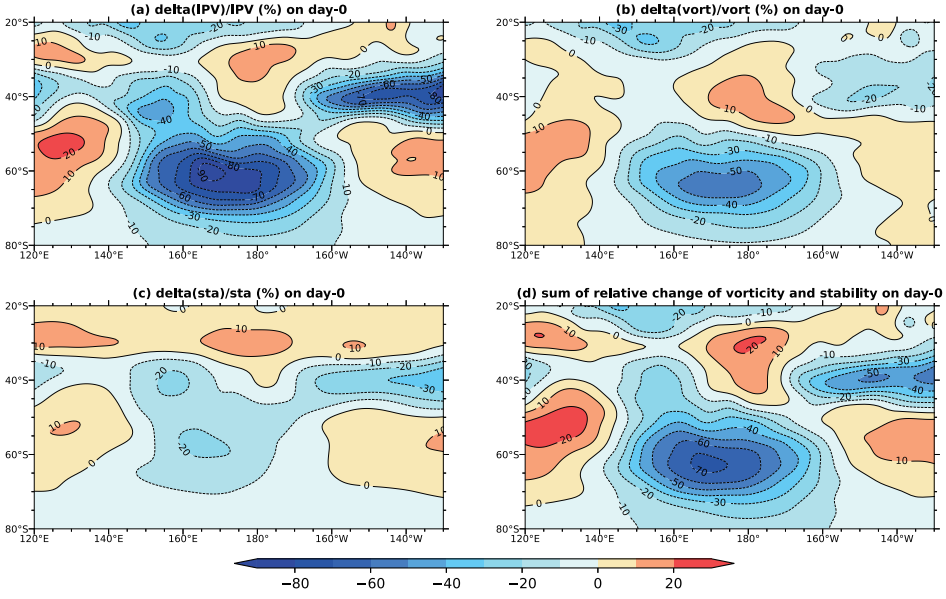

Figure 11. Same as in Fig. 10 except for the composite blocking events.

https://doi.org/10.5194/egusphere-2022-1038
Preprint. Discussion started: 6 October 2022

6 Static stability budget analysis

Given the local minimum of static stability accompanied with block onset, one may wonder what processes might cause it. Recall from the earlier discussion regarding the static stability tendency equation as shown in Eq. (6), a local change of static stability may be caused by horizontal or vertical advection of static stability through terms 1, 2 and 3 respectively. Moreover, static stability may be created or destroyed through vertical stretching or shrinking of an air column represented in term 4. That is, the horizontal convergence accompanied by stretching would move two isentropic surfaces farther apart and thus result in the decrease of static stability, while the horizontal divergence accompanied by shrinking would move two surfaces closer such that the static stability would increase. The differential diabatic heating, as in term 5, can also generate or destroy the static stability. In addition, in terms of contributions of diabatic heating to the static stability budget, term 5 and term 2 can be interpreted as the direct and indirect effects of diabatic heating, respectively.

Figure 12 illustrates the 6 hourly change of each term in the static stability tendency equation at 300 hPa isobaric surface on day-5 prior to block onset for the composite blocking cases. The day-5 was chosen here because each term of the static stability tendency equation features the most representative patterns during the 5-day pre-blocking period. The following results still hold regardless of which exact day was selected during the 5-day pre-blocking period. Figure 12 (a) shows the total static stability tendency and it is apparent that the block-onset region, particularly the upstream and poleward area, is characterized by decreasing static stability. Figure 12 (b) and (c) show the static stability tendency due to horizontal advection by the rotational and divergent wind, respectively. Both terms contribute to the decreasing static stability over the block-onset region, with the rotational component being the leading contributor and divergent component being the secondary contributor. Over the area characterized by the negative static stability tendency near block-onset region, the rotational wind is prevailingly southwesterly which advects low static stability into the block-onset region while the divergent wind generates convergence over the lower boundary of the block-onset region and divergence over the upper-left block-onset region, both leading to decreasing static stability. Figure 12 (d) shows that the vertical advection term opposes the advection term through enhancing the static stability over the middle and lower left block-onset region instead. The 300 hPa vertical velocity field in Fig. 12 (d) reveals that a strong sinking motion is dominant over the block-onset region such that it advects more stable air downward from the stratosphere thereby locally stabilizing the atmosphere column. Figure 12 (e) indicates the decreasing static stability tendency due to the stretching effect as the strong upper-level convergence field over the lower boundary of the block-onset region results in the stretching effect which locally destabilizes the air accordingly. Figure 12 (f) shows the direct effect of diabatic heating upon static stability tendency. In general, the equatorward side of the block-onset region is distinguished by decreasing static stability whereas the poleward side is dominated by increasing static stability. This is in contrast with the indirect effect of diabatic heating as shown in Fig. 12 (c) in which the block-onset region and the upstream region are entirely associated with decreasing static stability. In other words, the indirect effect of diabatic heating persistently favors the onset of blocking.

Table 2 and Table 3 list the calculated static stability tendency attributed to each term in the static stability budget, area-averaged over the block-onset region, for the July 1999 blocking case and the composite blocking cases, respectively, during the 5-day pre-blocking period and block onset day. The July 1999 blocking case demonstrates that the area-averaged total

https://doi.org/10.5194/egusphere-2022-1038
Preprint. Discussion started: 6 October 2022

analyzed static stability tendency is generally negative as block onset time approaches. In general, the horizontal advection effects, including rotational and divergent components, and stretching term both favor block onset by contributing decreasing static stability whereas the vertical advection term tends to oppose block onset with increasing static stability. The direct effect of diabatic heating persistently opposes block onset while the indirect effect of diabatic heating persistently favors block onset instead. The composite blocking results in Table 3 further strengthen these findings with more consistency among 5 days before block onset, except for the direct effect of diabatic heating, which is in small negative values implying favoring block onset. Nevertheless, since the magnitude of the direct effect of diabatic heating is nearly an order of magnitude smaller than other terms, its effect can be negligible. Instead, the indirect effect of diabatic heating stands out as one of the primary contributors to block onset.

https://doi.org/10.5194/egusphere-2022-1038
Preprint. Discussion started: 6 October 2022

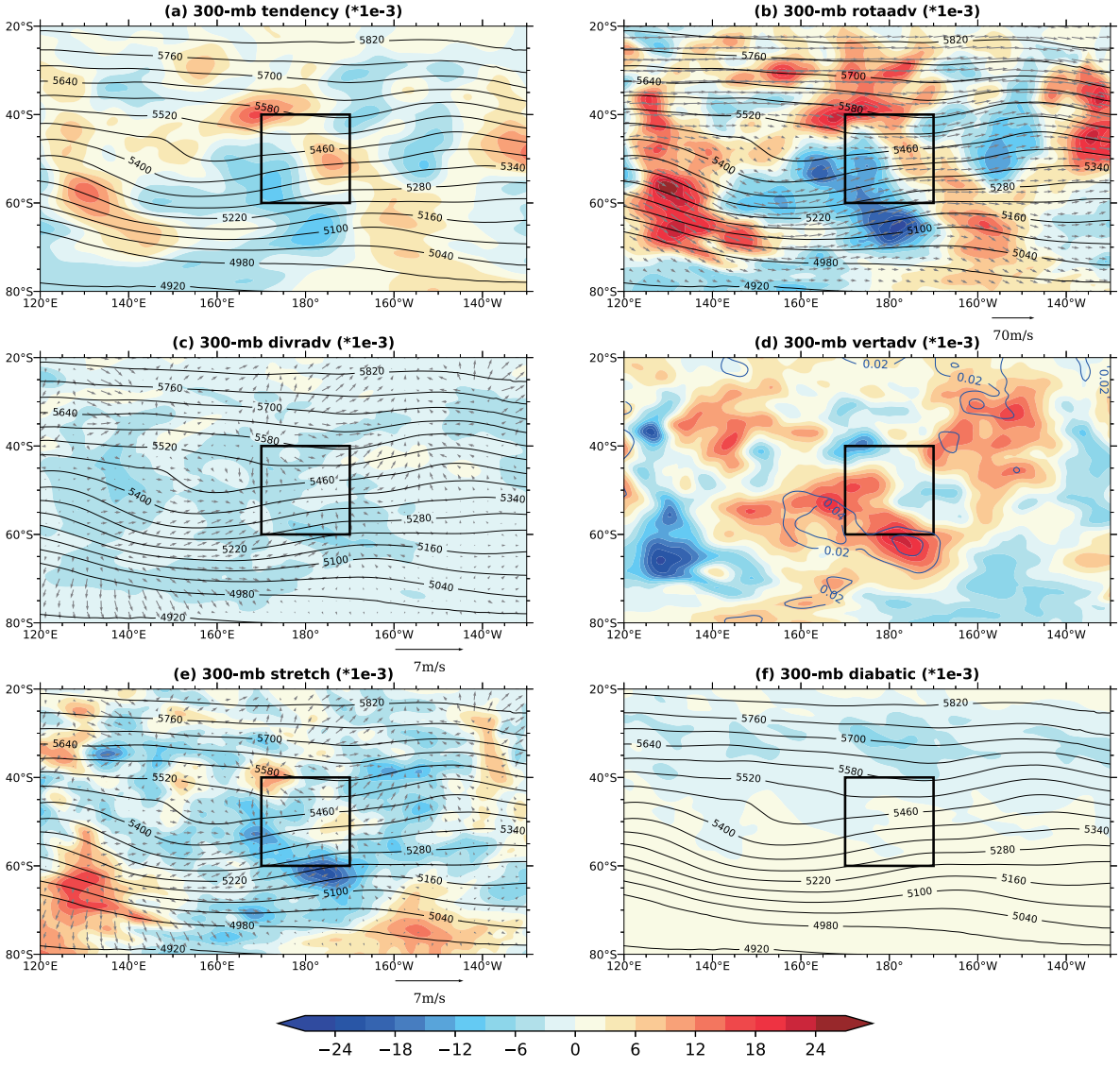

Figure 12. 300 hPa 6 h total static stability tendency (shaded) in (a), and resolved static stability tendency due to rotational wind advection (shaded) in (b), divergent wind advection (shaded) in (c), vertical advection (shaded) in (d), stretching term (shaded) in (e) and diabatic heating term (shaded) in (f), in units of 10^{-3} $\mathrm{m^2\ s^{-2}\ hPa^{-2}}$ $(6\ \mathrm{h})^{-1}$, for the composite blocking events on day-5 prior to block-onset day. The 500 hPa geopotential heights (contour) are overlaid in all subfigures except (d). The 300 hPa rotational wind vector is shown in (b), and divergent wind vector is shown in (c) and (e). The 300 hPa vertical velocity is shown in (d) in contour, in units of $hPa\ s^{-1}$. The composite pseudo block-onset region is highlighted in the black rectangle, which is centered at 180^o W.

https://doi.org/10.5194/egusphere-2022-1038
Preprint. Discussion started: 6 October 2022

Table 2. Calculated static stability tendency and each contribution term averaged over the block-onset region for the July 1999 blocking case.

July 1999 blocking case	Total tendency	Rotational	Divergent	Vertical	Stretching	Diabatic
Day-5	-22.6	-44.2	-4.3	30.0	-26.1	1.9
Day-4	-0.6	-16.8	-2.0	12.7	-8.5	2.8
Day-3	-3.1	-5.1	-1.3	5.2	-1.7	2.6
Day-2	-0.3	-2.7	-1.2	0.0	0.6	2.7
Day-1	5.0	7.0	-1.1	-0.6	2.3	2.1
Day-0	7.2	4.7	-2.5	2.1	2.1	1.5
6-day average	-2.4	-9.5	-2.1	8.2	-5.2	2.3

Table 3. Same as in Table 2 except for the composite blocking cases.

Composite blocking cases	Total tendency	Rotational	Divergent	Vertical	Stretching	Diabatic
Day-5	-2.4	-6.0	-3.8	6.6	-5.9	-0.3
Day-4	0.3	-4.8	-2.8	6.8	-4.6	-0.2
Day-3	-3.5	-8.8	-2.7	7.9	-6.4	-0.3
Day-2	-6.6	-10.7	-2.5	8.6	-6.9	-0.3
Day-1	-5.9	-11.0	-2.1	6.8	-5.2	-0.3
Day-0	0.8	-0.7	-1.7	4.6	-1.9	-0.1
6-day average	-2.9	-7.0	-2.6	6.9	-5.2	-0.3

As in Figure 12, Figure 13 presents the same terms in the static stability budget except in the form of area-average values from 700 hPa throughout 100 hPa. It is readily observed that within the upper-troposphere the total analyzed static stability tendency, horizontal advection term by the rotational and divergent wind, and the stretching term are generally distinguished by decreasing static stability whereas the vertical advection term is associated with increasing static stability. As for the direct effect of diabatic heating, the vertical profile tends to oscillate along the zero axis and its values are generally at least an order of magnitude smaller than other terms. Therefore, the aforementioned findings are once again confirmed.

https://doi.org/10.5194/egusphere-2022-1038
Preprint. Discussion started: 6 October 2022

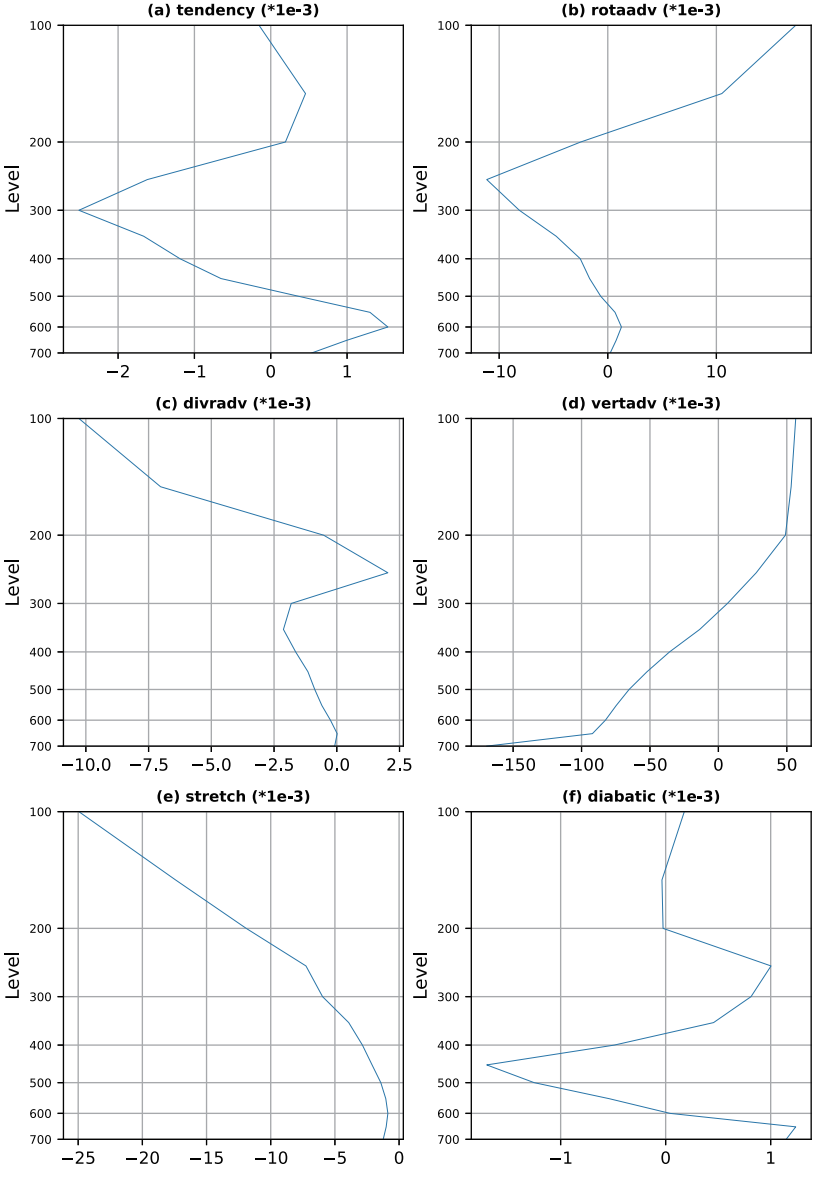

Figure 13. Same as in Fig. 12, except for the vertical profiles.

https://doi.org/10.5194/egusphere-2022-1038
Preprint. Discussion started: 6 October 2022

Based on Table 3, Fig. 14 provides a comparison between the total analyzed static stability tendency, i.e. the left hand side of Eq. (6), and the total calculated static stability tendency, i.e. the sum of the terms on the right hand side of Eq. (6) over the a 6 h interval, for the composite blocking cases during the 5-day pre-blocking period and the block-onset day. Generally speaking, the temporal evolution of the two quantities is reasonably similar. The discrepancies between the two quantities can be attributed to several reasons including comparing an instantaneous tendency with a finite-time difference and the omission of some subgrid-scale processes. Nevertheless, these discrepancies do not compromise the physical interpretations of our results. This is aligned with Teubler and Riemer (2016) who analyzed Rossby wave packets dynamics in terms of PV tendency equation and also found reasonable differences between their total analyzed and calculated PV tendencies.

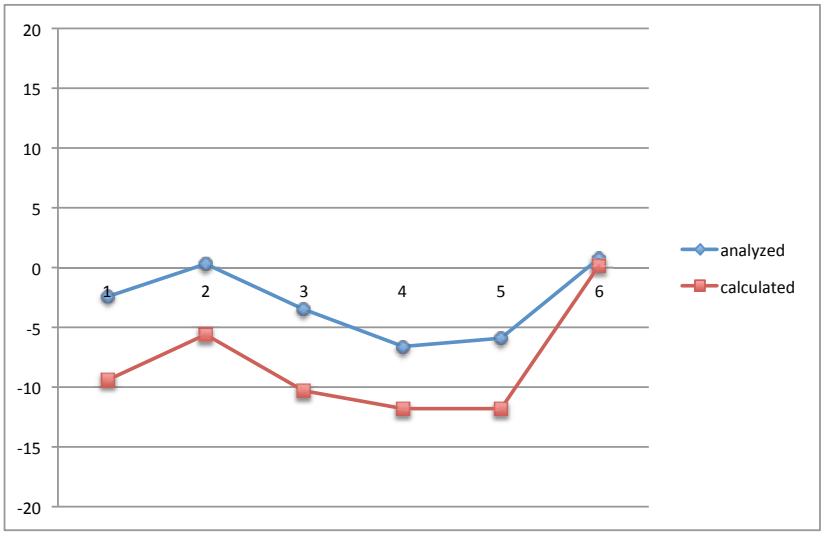

Figure 14. Comparison between total analyzed and calculated 6 h static stability tendency, in units of 10^{-3} $\mathrm{m^2\ s^{-2}\ hPa^{-2}\ (6\ h)^{-1}}$, for the composite blocking events during the 5-day pre-blocking period and the block-onset day. The x axis represents day-5, day-4, day-3, day-2, day-2, day-1 and block-onset day, from left to right.

https://doi.org/10.5194/egusphere-2022-1038
Preprint. Discussion started: 6 October 2022

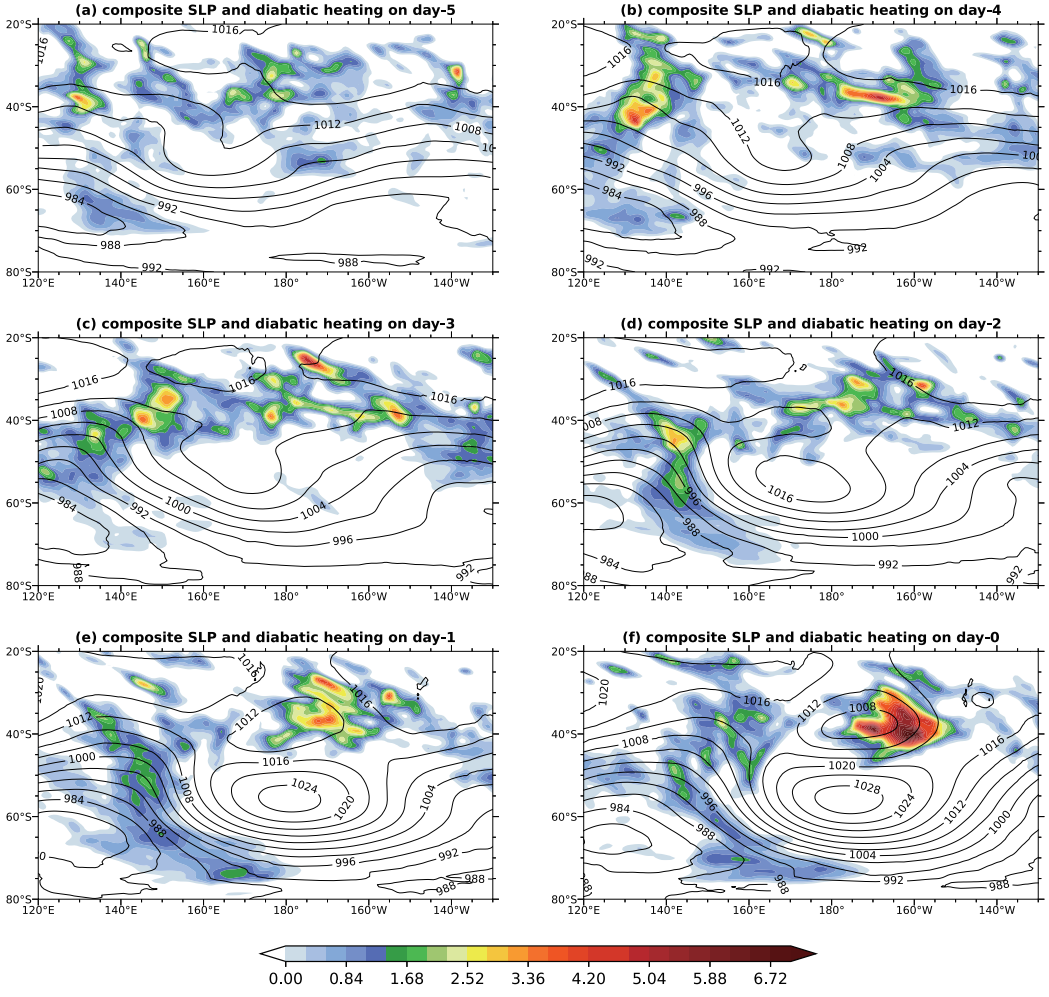

Figure 15. Sea level pressure (contour, in unit of hPa) and vertically averaged diabatic heating from 700 hPa to 500 hPa (shaded, in unit of K/day) for the composite blocking events during 5-day pre-blocking period and block-onset day.

In order to clearly depict the contributions of diabatic heating to static stability tendency, Fig. 15 shows the vertically averaged diabatic heating within 700-500 hPa overlaid over the sea level pressure field for the composite blocking events during the pre-blocking period. It is readily found that the diabatic heating is dominant over the surface cyclones upstream of block-onset region. This is consistent with previous studies that the cyclogenesis-associated latent heat release largely favors and contributes to the block onset (Colucci and Alberta, 1996). It is also consistent with studies on WCB of extratropical cyclones in that the intense ascending moist airflows over the WCB rise from lower troposphere into upper troposphere while moving polewards and this process generates significant amount of latent heating (Madonna et al., 2014; Wernli, 1997). In

https://doi.org/10.5194/egusphere-2022-1038
Preprint. Discussion started: 6 October 2022

particular, the indirect effect of diabatic heating, manifested as the advection of low PV (or small static stability) by the upper-tropospheric outflow resulting from the diabatic forcing, largely favors the block onset over the upstream of block-onset region, as shown in Fig. 12 (c). In addition, Fig. 15 also reveals that the diabatic heating release is dominant over the low pressure center equatorward of the blocking high center. This is also reflected in Fig. 12 (f) where the static stability tendency resolved into the direct diabatic heating effect is featured with negative values equatorward of block-onset region and positive values poleward side. In general, the indirect effect of diabatic heating outperforms the direct effect such that the overall effect of diabatic heating is favorable to block onset.

7 conclusions and discussion

Static stability is a fundamental dynamical quantity that defines the vertical temperature stratification of the atmosphere. In terms of blocking onset, static stability plays an important role in determining the stability of the atmosphere where baroclinic instability can be amplified and continue to grow. Most studies on block onset mechanisms are carried out from the perspective of isentropic potential vorticity, i.e. block onset is manifested as a low-PV anomaly. In fact, the change of PV is composed of two parts, namely the change of absolute vorticity and static stability. Nevertheless how much the contribution of static stability is to the low-PV anomaly formation accompanied with blocking onset is yet unknown. To the best of the authors' knowledge, so far no investigations have been done on block onset from the perspective of static stability. In the present study, we intend to better understand the nature of horizontal and temporal variability of static stability associated with blocking onset.

In this study, twenty representative blocking cases are selected from the SH blocking climatology objectively detected based on the combined AGP and APV blocking indices. The composite analysis shows that static stability in the upper troposphere and on the tropopause reached its local minimum over the block-onset region on the block-onset day, which is consistent with Smith and Tsou (1988) and Frederiksen (1982) who suggested that baroclinic disturbances are favored to grow in a relatively unstable atmosphere. The local minimum of static stability over block-onset region is also coincident with the local minimum of PV present in the same region. By partitioning the low-PV anomaly over the block-onset region into the absolute vorticity and static stability contributions, it is found that they account for roughly 70 % and 30 % of low-PV anomaly formation, respectively.

Through static stability budget analysis, we found that the horizontal advection of static stability is the leading contributor for destabilizing atmosphere over the block-onset region, i.e. the relatively low static stability over subtropics is advected poleward so as to decrease the static stability in the midlatitude. In addition, the stretching effect associated with upper-level convergence over block-onset region is found to destabilize atmosphere as well, with a relatively smaller magnitude compared to the horizontal advection contribution though. On the other hand, the vertical advection of static stability accompanied by the strong sinking motion in the upper troposphere is found to oppose the decreasing static stability as the sinking air tends to advect more stable air downward and hence stabilize the local air over the block-onset region. Our result is consistent with Teubler and Riemer (2016) who used a PV-potential temperature framework to analyze Rossby wave packets dynamics in that the dry-dynamics processes are key contributors to blocking onset and Rossby wave packets formations.

https://doi.org/10.5194/egusphere-2022-1038
Preprint. Discussion started: 6 October 2022

In terms of diabatic heating contribution to block onset, the direct effect is negligible given its magnitude is generally an order of magnitude smaller than other effects. Nevertheless, the indirect effect of diabatic heating, manifested as the advection of low PV (or low static stability) by the diabatically forced upper-tropospheric divergent outflow, largely favors the block onset by destabilizing the air over the upstream of block-onset region. Thus the overall effect of diabatic heating is favorable to the formation of block onset. This finding confirms the study of Pfahl et al. (2015); Steinfeld and Pfahl (2019) who revealed the importance of moist processes to blocking onset.

From a nonlinear barotropic vorticity equation, Shutts (1983) proposed a barotropic eddy straining mechanism by which the transient eddies are compressed in the region of time-mean diffluent flow and the eddies energy is given up to the blocking flow so as to maintain the blocking structure. In Shutts (1983), a wave maker is placed upstream of a stationary free Rossy wave of dipole structure such that it provides transient eddies to amply the Rossy wave and prevent the dipole blocking structure from being advected downstream by the mean westerly flow. Based on Mullen (1987), the wave maker of transient eddies should be located about a quarter wave length upstream of block-onset region. Here we may understand the wave maker as storm track or upstream cyclogenesis that is capable of generating transient eddies. According to the definition of the Eady growth rate, low static stability favors large Eady growth rate such that baroclinic eddies grow more rapidly in a more unstable atmosphere. Hence we would surmise that, over upstream block-onset region, the static stability field should be relatively low such that the wave maker generates baroclinic eddies more efficiently to maintain the blocking structure. This conjecture is in agreement with Penny et al (2010) who found that the Pacific midwinter suppression of storminess is due to the upstream high static stability over Asia which suppresses eddy generation and thus reduces seeding for the Pacific storm track. For the future work, we intend to verify this conjecture by performing a series of idealized numerical simulations in which static stability over the wave maker region will be altered so that we will be able to examine how this modulation would influence the onset timing for incipient blocking as well as blocking intensity.

https://doi.org/10.5194/egusphere-2022-1038
Preprint. Discussion started: 6 October 2022

Data availability.

The MERRA-2 data is made publicly available by GMAO at https://gmao.gsfc.nasa.gov/reanalysis/MERRA-2/. The algorithms for blocking detection and static stability budget computations are available to public upon request to Li Dong at Southern University of Science and Technology.

Author contributions. LD designed the study and wrote up the manuscript. HD performed case studies and prepared the majority of the figures. GS prepared data and helped with blocking detection. SJC provided guidance to this study and very constructive comments to the manuscript.

Competing interests. The authors declare that they have no conflict of interest.

Acknowledgements. This work was supported in part by grants from the National Natural Science Foundation of China (Grant No. 41975060) and Shenzhen Science and Technology Program (Grant No. JCYJ20190809163007701). Furthermore, we would like to acknowledge Joshua S. Watson from National Weather Service of NOAA for contributing the blocking detection results to us. Also we acknowledge NASA Global Modeling and Assimilation Office (GMAO) for providing The Modern-Era Retrospective analysis for Research and Applications, Version 2 (MERRA-2) data publicly.

https://doi.org/10.5194/egusphere-2022-1038
Preprint. Discussion started: 6 October 2022

References

Appenzeller, C. and Davies, H. C.: Structure of stratospheric intrusions into the troposphere, Nature, 358, 570–572, 1992.

Archambault, H. M., Bosart, L. F., Keyser, D., and Cordeira, J. M.: A climatological analysis of the extratropical flow response to recurving western North Pacific tropical cyclones, Mon. Wea. Rev., 141, 2325–2346, 2013.

Austin, J. F.: The blocking of middle latitude westerly winds by planetary waves, Quart. J. Roy. Meteor. Soc., 106, 327–350, 1980.

Barnes, E. A., Slingo, J., and Woollings, T.: A methodology for the comparison of blocking climatologies across indices, models and climate scenarios, Climatic Dynamics, 38, 2467–2481, 2012.

Bluestein, H. B.: Synoptic-Dynamic Meteorology in Midlatitudes, Vol. 1. Oxford University Press, 594pp, 1992.

Bosart, L. F. and Lackmann, G. M.: Post-landfall tropical cyclone reintensification in a weakly baroclinic environment: A case study of hurricane David (September 1979), Mon. Wea. Rev., 123, 3268–3219, 1997.

Colucci, S. J. and Alberta, T. L.: Planetary-scale climatology of explosive cyclogenesis and blocking, Mon. Wea. Rev., 124, 2509–2520, 1996.

Croci-Maspoli and Davies, H. C.: Key dynamical features of the 2005/2006 European winter, Mon. Wea. Rev., 137, 664–678, 2009.

Dong, L. and Colucci, S. J.: The role of deformation and potential vorticity in Southern Hemisphere blocking onsets, J. Atmos. Sci., 62, 4043–4056, 2005.

Duran, P. and Molinari, J.: Tropopause evolution in a rapidly intensifying tropical cyclone: a static stability budget analysis in an idealized axisymmetric framework, J. Atmos. Sci., 76, 209–229, 2019.

Eady, E. T.: Long waves and cyclone waves, Tellus, 1, 33–52, 1949.

Erler, A. R. and Wirth, V.: The static stability of the tropopause region in adiabatic baroclinic life cycle experiments, J. Atmos. Sci., 68, 1178–1193, 2011.

Frederiksen, J. S.: A unified three-dimensional instability theory of the onset of blocking and cyclogenesis, J. Atmos. Sci., 39, 969–987, 1982.

Frierson, D. M. W.: Robust increase in midlatitude static stability in simulations of global warming, Geophysical Research Letters, 33, DOI: 10.1029/2006GL027 504, 2006.

Frierson, D. M. W. and Davis, N. A.: The seasonal cycle of midlatitude static stability over land and ocean in global reanalyses, Geophysical Research Letters, 38, DOI: 10.1029/2011GL047 747, 2011.

Grams, C. M. and Archambault, H. M.: The key role of diabatic outflow in amplifying the midlatitude flow: a representative case study of weather systems surrounding Western North Pacific extratropical transition, Mon. Wea. Rev., 144, 3847–3869, 2016.

Grams, C. M., Wernli, H., Bottcher, M., Campa, J., Corsmeier, U., S. C. Jones, J. H. K., Lenz, C., and Wiegand, L.: The key role of diabatic processes in modifying the upper-tropospheric wave guide: a North Atlantic case-study, Quart. J. Roy. Meteor. Soc., 137, 2174–2193, 2011.

Grams, C. M., Jones, S. C., Davis, C. A., Harr, P. A., and Weissmann, M.: The impact of Typhoon Jangmi (2008) on the midlatitude flow. Part I: Upper-level ridgebuidling and modification of the jet, Quart. J. Roy. Meteor. Soc., 139, 2148–2164, 2013.

Green, J. S. A.: The weather during July 1976: some dynamical considerations of the drought, Weather, 32, 120–126, 1977.

Grise, K. M., Thompson, D. W. J., and Birner, T.: A global survey of static stability in the Stratoshere and Upper troposphere, J. of Climate, 23, 2275–2292, 2010.

Hoskins, B. J.: A potential vorticity view of synoptic development, Meteor. Appl., 4, 325–334, 1997.

https://doi.org/10.5194/egusphere-2022-1038
Preprint. Discussion started: 6 October 2022

Hoskins, B. J., Mclntyre, M. E., and Robertson, A. W.: On the use and significance of isentropic potential vorticity maps, Quart. J. Roy. Meteor. Soc., 111, 877–946, 1985.

Illari, L.: A diagnostic study of the potential vorticity in a warm blocking anticylone, J. Atmos. Sci., 41, 3518–3526, 1984.

Lupo, A. R. and Smith, P. J.: The interaction between a midlatitude blocking anticyclone and synoptic-scale cyclones that occurred during the summer, Mon. Wea. Rev., 126, 502–515, 1998.

Madonna, E., Wernli, H., and Joos, H.: Warm conveyor belts in the ERA-Interim dataset(1979-2010). Part I: Climatology and potential vorticity evolution, J. Climate, 27, 3–26, 2014.

Masato, G., Hoskins, B. J., and Woollings, T. J.: Wave-breaking characteristics of midlatitude blocking, Quart. J. Roy. Meteor. Soc., 138, 1285–1296, 2012.

Methven, J.: Potential vorticity in warm conveyor belt outflow, Quart. J. Roy. Meteor. Soc., 141, 1065–1071, 2015.

Mullen, S. L.: Transient eddy forcing of blocking flows, J. Atmos. Sci., 44, 3–22, 1987.

Nakamura, H., Nakamura, M., and Anderson, J. L.: The role of high- and low-frequency dynamics in blocking formation, Mon. Wea. Rev., 125, 2074–2093, 1997.

Nielsen-Gammon, J. W.: A visualization of the global dynamic tropopause, Bull. Amer. Meteor. Soc., 82, 1151–1167, 2001.

O'Gorman, P. A.: The effective static stability experienced by eddies in a moist atmosphere, J. Atmos. Sci., 68, 75–90, 2011.

Parker, T. J., Berry, G. J., and Reeder, M. J.: The influence of tropical cyclones on heat waves in Southeastern Australia, Geophys. Res. Lett., 40, 6264–6270, 2013.

Pelly, J. L. and Hoskins, B. J.: A new perspective on blocking, J. Atmos. Sci., 60, 743–755, 2003.

Pfahl, S., Schwierz, C., Croci-Maspoli, M., Grams, C. M., and Wernli, H.: Importance of latent heat release in ascending air streams for atmospheric blocking, Nature Geosci, 8, 610–614, 2015.

Quinting, J. and Reeder, M.: Southeastern Australian heat waves from a trajectory viewpoint, Mon. Wea. Rev., 145, 4109–4125, 2017.

Rex, D. F.: Blocking action in the middle troposphere and its effect upon regional climate. I. An aerological study of blocking action, Tellus, 2, 196–211, 1950.

Riemer, M., Jones, S. C., and Davis, C. A.: The impact of extratropical transition on the flow: An idealized modeling study with a straight jet, Quart. J. Roy. Meteor. Soc., 134, 69–91, 2008.

Schwierz, C., Croci-Maspoli, M., and Davies, H. C.: Perspicacious indicators of atmospheric blocking, Geophys. Res. Lett., 31, L06 125, 2004.

Shutts, G. J.: The propagation of eddies in diffluent jetstreams: Eddy vorticity forcing of "blocking" flow fields, Quart. J. Roy. Meteor. Soc., 109, 737–761, 1983.

Smith, P. J. and Tsou, C.-H.: Static stability variations during the development of an intense extratropical cyclone, Mon. Wea. Rev., 116, 1245–1250, 1988.

Steinfeld, D. and Pfahl, S.: The role of latent heating in atmospheric blocking dynamics: a global climatology, Climatic Dynamics, 53, 6159–6180, 2019.

Swanson, K. L.: Blocking as a local instability to zonally varying flows, Quart. J. Roy. Meteor. Soc., 127, 1341–1355, 2001.

Teubler, F. and Riemer, M.: Dynamics of Rossby wave packets in a quantitative potential vorticity-potential temperature framework, J. Atmos. Sci., 73, 1063–1081, 2016.

Tibaldi, S. and Molteni, F.: On the operational predictability of blocking, Tellus, 42, 343–365, 1990.

https://doi.org/10.5194/egusphere-2022-1038
Preprint. Discussion started: 6 October 2022

Tsou, C.-H. and Smith, P. J.: The role of synoptic/planetary scale interactions during the development of a blocking anticyclone, Tellus, 42, 174–193, 1990.

Watson, J. S. and Colucci, S. J.: Evaluation of ensemble predictions of blocking in the NCEP global spectral model, Mon. Wea. Rev., 130, 3008–3021, 2002.

Wernli, H.: A Lagrangian-based analysis of extratropical cyclones. II: A detailed case-study, Quart. J. Roy. Meteor. Soc., 123, 1677–1706, 1997.

Wernli, H. and Davies, H.: A Lagrangian-based analysis of extratropical cyclones. I: The method and some applications, Quart. J. Roy. Meteor. Soc., 123, 467–489, 1997.

Wernli, H. and Sprenger, M.: Identification and ERA-15 climatology of potential vorticity streamers and cutoffs near the extratropical tropopause, J. Atmos. Sci., 64, 1569–1586, 2007.